Stabilization of atoms in ultrastrong laser fields: A classical approach

Mariusz Gajda,* Jan Grochmalicki, Maciej Lewenstein,
and Kazimierz Rzążewski
Institute for Theoretical Physics, Polish Academy of Sciences, 02-668 Warsaw, Poland
(Received 4 December 1991)

We study the classical theory of the response of atoms to ultrastrong laser pulses. We argue that the stabilization of atoms in a strong laser field through bound states in a Kramers-Henneberger potential has a classical interpretation. We present results of numerical simulations based on a phase-space-averaging method for a one-dimensional smoothed potential, which agree very well with the results of quantum theory. In a three-dimensional Coulomb potential, classical simulations hardly allow for stabilization, in contrast to recently obtained quantum-mechanical results. We identify physical reasons for this discrepancy with the effect of smoothing the potential singularity. We stress the relevance of our studies in the context of the correspondence principle.

PACS number(s): 32.80.Rm, 42.50.Hz

I. INTRODUCTION

Relations between classical and quantum dynamics and the role of the correspondence principle [1] have been studied very widely over the years. The notion of dynamical chaos in classical systems warrants the question of behavior of the underlying quantum systems (cf. [2]). The most interesting experimental verification of the predictions of both theories in atomic physics is offered by the interaction of atomic hydrogen in the Rydberg level with a linearly polarized microwave field. Both analogies and sharp differences are found (cf. [3–5]).

While nobody expects that the classical dynamics is a qualitatively good description of the interaction of the strong electromagnetic field with the atom in its ground state, there are a number of papers which conduct such a study [6–10]. Properties of the spectra of liberated electrons, the so-called above-threshold ionization [11], consisting of series of maxima separated by the single-photon energy are not reproduced well by classical physics. On the other hand, properties of the higher harmonics of light generated in the interaction of a very intense pulse with an atom are qualitatively similar to the corresponding quantum results [12]. Of course, the former requires the Planck constant to define the energy of a single photon, while the latter only the frequency of the light, a purely classical concept.

Series of recent papers discuss an intriguing possibility of stabilization of atoms in a very intense laser field. According to these papers [13, 14], in the limit of high frequency, asymptotically stable levels of the atom distorted by the field are formed. The ionization rate is not a monotonically growing function of the light intensity, and beyond a certain value, which is close to the characteristic atomic intensity (3.51×10^{16} W/cm^2) starts to decrease. The early papers assumed that the strong field is a continuous wave. The reality, however, is very different and the very strong field may only be produced in a form of very short pulses. It is not obvious that one can *introduce* the atom intact into this field. Hence, the response of the atom to such a pulse, a truly time-dependent dynamical problem, should be studied. The first demonstration that the atom could survive the strong pulse [15] was done with the help of a one-dimensional model. Other studies [16] confirmed this and stressed the usefulness of the so-called, Kramers-Henneberger frame of reference [17]. However, the real atoms are three-dimensional (3D) and the very different geometric properties of the phase space call for the studies in 3D.

In our recent Letter [18] we stressed that the basic mechanism of stabilization discovered by Gavrila and Kamiński [14] is classical in nature. So the classical dynamics, less demanding numerically, could in principle help to check if there is a substantial difference between one- and three-dimensional cases. After establishing good correspondence between classical and quantum results in 1D, we went on to simulate the response of the 3D hydrogen atom to a short laser pulse. We discovered that finding stabilization requires much higher frequency in this case. However, soon 3D quantum calculations were published [19] with the conclusion that the stabilization in 3D is even easier than in 1D. This conclusion is in contrast with the new paper of You, Mostowski, and Cooper [20]. This last paper studies one- and two-dimensional models both classically and quantum mechanically. While quantum physics predicts stabilization in both cases, the effect is weaker in the two-dimensional potential and the ionization probabilities are higher. Corresponding classical simulations overestimate the ionization probabilities substantially. The lack of quantum-classical correspondence is in this case hardly surprising as the authors study the short-range potential which supports only one bound state, i.e., the system which does not have a classical analog.

The purpose of this paper is to investigate further the classical dynamics of a strongly driven atom under conditions that lead to stabilization in the quantum-mechanical case. We look closer into dynamical behavior of the atom *during* interaction for 1D and 3D models. For the 3D Coulomb potential we find that two com-

pletely different regimes of dynamics may be identified: the switching regime, when most of the energy is absorbed, and the plateau regime, when absorption rate is very small. The dramatically higher classical ionization probabilities are entirely due to this switching part of the evolution. We further study the regularized Coulomb potential and find strong stabilization there [21]. This suggests that the principal quantum effect in the dynamics of 3D hydrogen consists in effective smoothing of the Coulomb singularity. We present angular distributions of outgoing electrons and find signatures of stabilization there. We comment on the relevance of our classical simulations for the studies of Rydberg states. Although results analogous to ours have been also discussed by other authors, who studied classical theory of ionization [6, 7, 22, 4], our paper connects a traditional view on this problem with the approach based on the Kramers-Henneberger method.

The plan of the paper is the following: in Sec. II we discuss once more the effect of stabilization, and present its classical interpretation. Section III contains a short reminder of various versions of the phase-averaging method [6, 7]. In Sec. IV we present results for the 1D model, stressing the role of the Kramers-Hennenberger potential and the correspondence to the quantum-mechanical case. We show also that in the classical case the signatures of stabilization can be seen for much lower values of the field than those corresponding to the splitting of the effective potential into two wells. Section V contains 3D results obtained for a pure Coulomb potential. Stabilization is in general hardly observed for this case. In Sec. VI we present results for a regularized Coulomb potential, and find strong stabilization there. The paper ends with conclusions concerning possible interpretation of our results in the context of quantum-classical correspondence.

II. STABILIZATION OF ATOMS IN VERY INTENSE LASER FIELDS

In some situations, a forced fast oscillations may be employed to turn the otherwise unstable configuration of the system into the stable one [23]. Recently, Gavrila and his co-workers suggested [14] that the effect of this kind should also appear in the high-frequency strong-field ionization. For the laser field frequency ω_L sufficiently high, its further increase should lead to a substantial suppression of the ionization, even for ultrastrong intensities. Stabilization has quickly become a major topic of the physics of intense laser-atom interactions, and there is already a topical meeting devoted only to this phenomenon [24].

The effect of stabilization was discovered by Gavrila and his collaborators in the framework of quantum mechanics, by means of the so-called Kramers-Henneberger (KH) transformation [17] (the space-translation method), which transfers the rapid oscillations of the external field to the atomic potential. Then, by averaging over these oscillations, one finds an effective double-well potential, describing atoms in the high-frequency laser field. Furthermore, it turns out that the usual ground state of the atom undergoes "dressing" in such a potential, and is stable against the ionization not only when the laser frequency ω_L, but also when the laser intensity, grows. Due to the double-well character of the effective potential, wave function of the electron trapped in the ground state becomes *dychotomic*.

Immediately, the above prediction has been criticized, since the described approach ignores the effects connected with introducing the atoms into the oscillating field, and assumes the ideal plane-wave form of the field, rather than a pulse form. Also, as pointed out by Lambropoulos [25], any nonperturbative strong-field effects can hardly be observed in ionization by typical laser pulses. Full ionization takes place in the initial growth phase of the pulse, when the field is still in the perturbative regime. No further absorption or emission processes by the released electron are then possible in the developed intense plane-wave field. Obviously, such criticism does not apply, if the turn-on time is sufficiently short.

To resolve the above controversy Eberly and co-workers [15] investigated numerically Schrödinger equation describing the one-dimensional model atom under the influence of a short laser pulse, controlling the turn-on and turn-off times of the pulse. For sufficiently rapid turnon they observed stabilization of the atom, i.e., the decrease of the ionization probability. This result shows that a nondestroyed atom can indeed enter into the region of strong field. The results of Su, Eberly, and Javanainen [15] have been recently confirmed by Reed, Knight, and Burnett [16], who performed a careful analysis of the 1D model in the KH frame. They showed that the wave function of the trapped electrons have a *polytomic*, rather than *dychotomic* character. That might indicate that electrons are not trapped in the ground state of the KH potential, but instead in a mixed combination of several bound states [26]. Kulander, Schafer, and Krause [19], using massive computing power, presented evidence for stabilization in three-dimensional fully quantum calculations for a hydrogen atom. A similar conclusion has been obtained in quantum calculations of You, Mostowski, and Cooper [20], who studied a two-dimensional hydrogen atom.

We have demonstrated [18] that the aforementioned effect of atomic stabilization has a purely classical counterpart, and that the degree of stabilization depends critically on the dimensionality of the phase space. We showed that the significant stabilization is reproduced in the classical version of the one-dimensional model atom of Eberly and co-workers [27], interacting with short superintense laser pulses. Then, we provided evidence that according to classical mechanics such an effect should be substantially reduced for true three-dimensional atoms.

In order to understand the stabilization of the atom in classical terms, we consider an electron in the Coulomb potential V_{Coul} in the field of a plane wave of frequency ω_L. The classical (nonrelativistic) equations of motion, in the dipole approximation, are

$$\frac{d}{dt}\mathbf{x} = \mathbf{v}, \tag{1}$$

$$m\frac{d}{dt}\mathbf{v} = -\nabla V_{\mathrm{Coul}} + e\boldsymbol{\mathcal{E}}_L \sin(\omega_L t), \tag{2}$$

where $\mathcal{E}_L$ is the amplitude of the electric field. The classical Kramers-Henneberger transformation consists in changing the laboratory frame to the one that follows the classical motion of an electron in the plane-wave field, $\mathbf{x} = \mathbf{y} - (e\mathcal{E}_L/m\omega_L^2)\sin(\omega_L t)$, $m\frac{d}{dt}\mathbf{y} = \boldsymbol{\pi}$, so that

$$\frac{d}{dt}\boldsymbol{\pi} = -\boldsymbol{\nabla} V_{\text{Coul}}\left(\mathbf{y} + \frac{e\mathcal{E}_L}{m\omega_L^2}\sin(\omega_L t)\right). \tag{3}$$

For large ω_L the potential in Eq. (3) may be replaced by its average V_{eff} [17]

$$V_{\text{eff}}(\mathbf{y}) = \frac{\omega_L}{2\pi}\int_0^{2\pi/\omega_L} dt V_{\text{Coul}}\left(\mathbf{y} + \frac{e\mathcal{E}_L}{m\omega_L^2}\sin(\omega_L t)\right). \tag{4}$$

Note that $V_{\text{eff}}(\mathbf{y})$ is time independent, and has typically two attraction centers, at $\pm e\mathcal{E}_L/m\omega_L^2$. We denote in the following the classical excursion amplitude $\alpha \equiv |e\mathcal{E}_L/m\omega_L^2|$. The corrections to $V_{\text{eff}}(\mathbf{y})$ (the higher-order Fourier components) are rapidly oscillating functions of time. The effective potential can be easily calculated for the one-dimensional model atom, as discussed in Refs. [16, 27]. Such a model corresponds to a regularized Coulomb potential $V_{\text{reg}}(x) = -1/\sqrt{1+x^2}$. The amplitude of the lowest-order correction to the potential $V_{\text{reg}}(x)$ decreases as a function of ω_L, and saturates as a function of I. Therefore, the overall impact of the correction remains negligible. The same conclusion holds also in three dimensions, $D = 3$.

The classical stabilization of an atom can be explained as follows. A classical phase-space distribution of electrons that mimics the quantum ground state in the potential V_{eff} will be concentrated in configuration space around the two minima of V_{eff}, and, hence, will be dychotomic. After transforming it back to the laboratory frame, such a distribution will oscillate with the frequency ω_L. Its zeroth Fourier component describes the effective distribution of particles (i.e., the distribution that measures how often a given region of configuration space is visited by particles from the sample). Obviously, such an effective distribution will have three peaks, with symmetric maxima at $\mathbf{x} = \pm 2e\mathcal{E}_L/m\omega_L^2$, and a maximum around $\mathbf{x} = \mathbf{0}$ that is roughly twice as large. Thus, for such distribution nearly half of the population will be frequently very close to the Coulomb force center, having low momentum, and may remain trapped after the field is rapidly turned off.

The above statements can be formulated also in the quantum theory, provided that we apply them to the wave functions rather than to the probability distributions in the configuration space. In this case, however, the additional quantum interference effects are possible. They can limit the validity of our classical argument.

We have verified the above heuristic arguments using the classical simulation of the ionization process. Such an approach was introduced by Leopold and Percival [6, 7], and is widely known as a phase-space-averaging method. Here, the quantum-mechanical initial state of an atom is approximated by an initial data distribution (being, for instance, a microcanonical ensemble, constructed using the reversion of the Einstein-Brillouin-Keller quantization scheme). Various versions of this method used by us are described in the next section. Here, we just stress that our simulations in 1D not only showed that stabilization in the KH frame can be explained classically. Moreover, they exhibited amazing agreement with the quantum-mechanical results of Su, Eberly, and Javanainen [15]. In fact, recently Grobe and Law [28] performed a very careful comparison between quantum and classical results in 1D and confirmed our earlier observations. On the other hand, we have presented evidence that the effect of stabilization will be substantially reduced for true three-dimensional, but classical atoms. For such atoms, the phase-space geometry allows for much more complex motions of electrons. This property of the phase space accompanied, for yet stronger intensities, by relativistic effects, makes the significant stabilization hardly possible. This classical result stands in contrast to quantum-mechanical results of Kulander and co-workers [19]. In the next section we shall provide more insight into the classical results in 1D and 3D, and try to understand the reasons for a very good and a very bad quantum-classical correspondence in these two cases, respectively.

III. PHASE-SPACE AVERAGING METHOD AND ITS APPLICABILITY

The phase-space-averaging method has been introduced by Leopold and Percival [6, 7, 29] to describe the response of highly excited atoms and molecules to low-frequency laser or maser radiation. The motivation for the method comes from the correspondence principle. It is obvious that highly excited states of atoms and molecules (such as Rydberg states of hydrogenlike atoms) may form wave packets [30] that have to a great extent classical character. The dynamics of such packets under the influence of an external, low-frequency field may also be described by means of classical mechanics. The dominant effect of quantum fluctuations in such a process enters through the fact that initial states in most of the situations of interest are not a wave packet. Instead, it is typically a state of well-defined energy, which is not localized in the phase space. To describe this situation, Leopold and Percival proposed to mimic the quantum-mechanical initial state by the statistical sample of initial points in the phase space. The results of quantum measurements (quantum-mechanical averages) are then identified with the averages over the sample of initial data. For instance, the degree of ionization (after termination of the laser pulse), is determined as a fraction of the sample with positive final energies (fraction of unbounded electrons).

The phase-space-averaging method has proved to be very fruitful for a description of microwave ionization of highly excited hydrogen atoms [6, 7, 3, 22, 4]. Mostowski and Życzkowski [8] proposed to extend it to describe strong-field above-threshold ionization (ATI) of atoms [11]. Here typically the initial state corresponds rather to a ground state, while the driving field may have optical

or even higher frequency. One expects, however, that for very strong fields the role of quantum fluctuations will again be essential only initially. The application of the method in the context of ATI has led to a number of valuable qualitative and quantitative results [9, 10, 12].

The construction of the sample of initial data may be performed in various ways. We have used in our simulation two methods:

• *Ensemble I.* This is a microcanonical ensemble proposed by Leopold and Percival and constructed as a reversion of the Einstein-Brillouin-Kramers quantization scheme (for details see also [10]). One introduces here action-angle variables [23, 31] and constructs the sample by fixing the actions and taking the conjugated angles to be uniformly distributed. For hydrogen atom with fixed energy $E < 0$ and angular momentum L, in practice, this aim may be achieved by the following steps: (a) we choose a random unit vector that determines the direction of angular momentum, i.e., the plane of the motion; (b) the motion on that plane follows an elliptical trajectory and may be parametrized using the parameter ξ [23]:

$$r = a(1 - e\cos\xi), \tag{5}$$

$$t = \sqrt{a^3}(\xi - e\sin\xi), \tag{6}$$

where $a = 1/2|E|$ denotes half of the large axis of the ellipse, whereas $e = L/\sqrt{2|E|}$ is its eccentricity; (c) the spatial distribution on that plane and the corresponding distribution of momenta corresponds to a uniform distribution of times t on the interval equal to the period of the motion, $T = t(2\pi) - t(0) = 2\pi\sqrt{a^3}$. To perform a Monte Carlo sampling one has in principle to invert the transcendental relations (6). Note, however, that the marginal radial distribution can be obtained analytically,

$$f(r) = \frac{\sqrt{a}r}{\sqrt{a^2e^2 - (r-a)^2}}. \tag{7}$$

• *Ensemble II.* An alternative construction of the microcanonical ensemble is performed as follows. We consider spherical coordinates and canonical variables, r, θ, ϕ, and conjugated momenta p_r, p_θ, p_ϕ. The microcanonical ensemble corresponds to the fixed values of E, L and z component of the angular momentum L_z,

$$\rho(r,\theta,\phi,p_r,p_\theta,p_\phi) = \mathcal{N}\delta\left(\frac{1}{2}\left[p_r^2 + \frac{1}{r^2}\left(p_\theta^2 + \frac{p_\phi^2}{\sin^2\theta}\right)\right] - \frac{1}{r} + |E|\right) \times\delta\left(p_\theta^2 + \frac{p_\phi^2}{\sin^2\theta} - L^2\right)\delta(p_\phi - L_z), \tag{8}$$

where $\mathcal{N}$ is a normalization constant. Integrating Eq. (8) over ϕ, and all of the momenta, we obtain the marginal distribution of r and θ,

$$f(r,\theta) \propto \frac{r}{\sqrt{r - |E|r^2 - L^2/2}} \frac{1}{\sqrt{L^2 - L_z^2/\sin^2\theta}}. \tag{9}$$

It is elementary to check that the resulting marginal radial distribution is the same as the one given by expression (7). Note that θ is statistically independent of r, and its marginal distribution is given by the second factor on the right-hand side of Eq. (9). The construction of a spherically symmetric sample that corresponds to a ground state of the hydrogen ($E = -\frac{1}{2}$) can be performed in the following steps: (a) we choose $r \in [r_{\min} = L^2/2, r_{\max} = 2 - L^2/2]$ in accordance with the distribution (7). Note that L^2 must be smaller than $-1/(2E)$, i.e., $0 \le L \le 1$ for $E = -\frac{1}{2}$; (b) we choose a random $L_z = p_\phi$, uniformly distributed in the interval $[-L, L]$; (c) we calculate $p_r = 2(E + \frac{1}{r}) - \frac{L^2}{r^2}$; (d) we choose $\theta \in [\arcsin(L_z/L), \pi - \arcsin(L_z/L)]$, in accordance with the distribution (9); (e) we calculate $p_\theta = \sqrt{L^2 - L_z^2/\sin^2\theta}$; (f) finally, we choose a random ϕ, uniformly distributed in the interval $[0, 2\pi]$. A nice feature of this construction is its applicability to any central potential.

In the following we have used both equivalent constructions alternatively, and assumed various values of the angular momentum L. In 1D both constructions become the same. In all simulations we have used samples of between 500 to several thousand trajectories, depending on the required accuracy of the averaging procedures.

The phase-space-averaging method, as we mentioned, was primarily designed to describe microwave excitation of Rydberg atoms. This is a situation when driving pulses are very long and adiabatically turned on and off. The classical dynamics in such a case is determined by asymptotic (long-time) properties of the phase space (periodic and/or chaotic orbits [6, 7, 22]). Such classical description remains valid provided there is not enough time for quantum-interference effects to exhibit themselves [3, 4]. This may happen only if the initial states are sufficiently "classical" in character, i.e., are highly excited Rydberg states.

The situation is drastically different in the regime of strong-field optical excitation. Here, we deal with very short pulses, and for very intense fields the relevant dynamics takes part sometimes during a couple of optical cycles. For the pulse, the electric field in Eq. (1) has to be taken in the form

$$\mathcal{E}_L(t) = \mathcal{E}_L f(t)\sin(\omega_L t + \phi). \tag{10}$$

We have been working with various envelope functions, such as a trapezoidal one,

$$f(t) = \begin{cases} t/T_{\text{on}} & \text{for } 0 \le t \le T_{\text{on}} \\ 1 & \text{for } T_{\text{on}} \le t \le T_D - T_{\text{off}} \\ 1 - (t - T_D + T_{\text{off}})/T_{\text{off}} & \text{for } T_D - T_{\text{off}} \le t \le T_D. \end{cases} \tag{11}$$

$T_{\rm on}$, $T_{\rm off}$ describe here the turn-on and turn-off times of the pulse, respectively, and ϕ is the phase. Pulse duration is of course denoted as T_D. Alternatively, we have used sinusoidal pulses,

$$f(t)=\begin{cases}\sin^2(\pi t/2T_{\rm on}) & \text{for } 0\le t\le T_{\rm on}\\ 1 & \text{for } T_{\rm on}\le t\le T_D-T_{\rm off}\\ \sin^2[\pi(t-T_D+2T_{\rm off})/2T_{\rm off}] & \text{for } T_D-T_{\rm off}\le t\le T_D.\end{cases}\tag{12}$$

When the excitation is induced by a pulse we may hope that dynamical quantum-interference and quantum-diffusion effects may remain negligible, even if we start from the ground state; quantum aspects may be fully accounted for via phase-space averaging. This belief finds additional support if we take into account the fact that short excitation pulses themselves exhibit fluctuations (i.e., intensity or phase fluctuations) that may smooth out quantum effects completely [10]. We will present some results that correspond to such averaging, but we shall also focus on the response of atoms to pulses that have fixed phase ϕ and fixed intensity. This will allow us to discuss specific aspects of the atomic response, such as a role of pulse area and thus induced drift forces. We stress, however, that in any case the classical problem that we study is a transient one. The response of atoms in such a case will therefore be determined not only by asymptotic properties of the phase space, but also by transient phenomena, such as unstable orbits and transient chaos.

On the other hand, it is well known that classical dynamics of the hydrogen atom in the plane wave exhibits scaling. Namely, if we introduce a scaling parameter n (an analog of the principal quantum number) the equations of motion are invariant with respect to the transformation

$$E\to(1/n^2)E,\tag{13}$$

$$\omega_L\to(1/n^3)\omega_L,\tag{14}$$

$$\mathcal{E}_L\to(1/n^4)\mathcal{E}_L.\tag{15}$$

The scaling means that the results that correspond to ionization from the ground state may easily be translated into results that correspond to the ionization from the nth Rydberg state. In particular, the scaling (15) may be extended to the case of pulse excitation, provided we keep constant the ratio of T_D, $T_{\rm on}$, and $T_{\rm off}$ to the optical period. The additional scaling relations are therefore (each of the T's scales as inverse of ω_L),

$$T_D\to n^3T_D,\tag{16}$$

$$T_{\rm on}\to n^3T_{\rm on},\tag{17}$$

$$T_{\rm off}\to n^3T_{\rm off}.\tag{18}$$

This fact has very important experimental consequences, since it is much more easier to achieve the required intensities for the light sources working in infrared and optical regimes, rather than those working in the ultraviolet domain. It suggests also that our results have a very broad domain of applications.

The doubts about applicability of phase-space-averaging methods come from the fact that although it does mimic some quantal aspects of the motion, it definitely is not sufficient. There have been attempts, therefore, to replace the phase-space-averaging method by a more accurate one. One way consists in the use of a quasiprobability approach [32, 33]. Such an approach is, in principle, equivalent to a full quantum-mechanical theory, but has the following drawbacks:

- Most of the quasiprobabilities, such as Wigner function [34], or Glauber's P representation [35], are not positively defined. If one tries to overcome this difficulty by taking an absolute value or using positively defined functions such as a Q representation [35] or a Husimi function [36] another problem arises. Typically, such a representation of the ground state or other bound states of an atom contains, from the very beginning, a fraction of electrons that are ionized in the classical sense (i.e., have positive energy) [37]. This fraction ranges typically from 10 to 20%. Such a representation cannot therefore allow for a description of ionization at a low level. On the other hand, when ionization probability is between 0.5 and 1 (which is typical in the problems of stabilization), we think that the quasiprobability method might prove useful.

- Quasiprobability functions undergo much more complex dynamics than classical phase-space densities (considered in the phase-space-averaging method). Roughly speaking, quantum fluctuation and interference effects are present not only in the description of the initial state, but also during the evolution. It is not clear how one could easily incorporate these effects.

IV. STABILIZATION IN 1D REGULARIZED POTENTIAL

In this section we present results obtained from classical simulation of the one-dimensional model. We use the same potential as the one introduced by Su , Eberly, and Javanainen [15]

$$V(x)=-1/\sqrt{x^2+\epsilon^2}.\tag{19}$$

As pointed out by Javanainen, Eberly, and Su [27], this potential has a lot in common with the 3D Coulomb potential; it has Rydberg series, it has an additional, besides principal, discrete quantum number, i.e., parity. The potential is regularized at $x=0$. The necessity of regularization follows in the first place from the requirement of mathematical consistency. The radius of regularization has been chosen by the authors to be 1. This has a nice physical explanation, since this choice leads to a ground-state energy of the 1D model roughly equal to that of the 3D hydrogen atom, $E=-0.668\simeq-0.5$. We think that in fact the regularization procedure of Su, Eberly, and

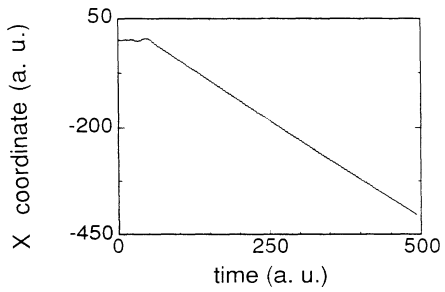

FIG. 1. Trajectory of an electron (x coordinate) ionized in the regularized 1D potential as a function of time. The laser pulse has a sinusoidal shape with $\mathcal{E}_L = 5$, $\omega_L = -2E$, $\omega_L T_{\rm on}/2\pi = 5$, $\omega_L T_D/2\pi = 105$, and $\omega_L T_{\rm off}/2\pi = 5$. The initial phase of the pulse has been chosen randomly. All quantities are in atomic units.

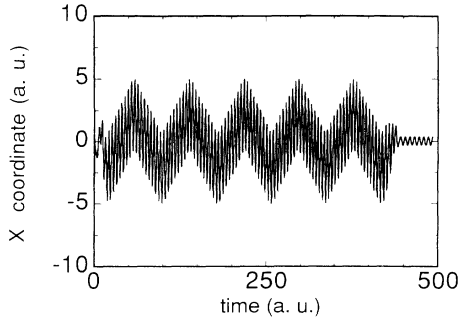

FIG. 3. Trajectory of an electron (x coordinate) trapped in the regularized 1D potential as a function of time. Parameters are the same as in Fig. 1.

Javanainen has an even deeper physical meaning. Our classical analysis indicates that regularization is essential for stabilization. One-dimensional models that are designed in order to mimic three-dimensional quantum physics have to be regularized [38]. If they were not, they would not lead to stabilization, which is observed in 3D quantum models [19].

The results that we present in this section concern the character of stabilization in 1D and the relevance of the Gavrila mechanism. Our results may be considered as complementary to those of Grobe and Law [28], who have recently performed a careful analysis of the quantum-classical correspondence in the 1D models with the potential (19).

As has been shown in our Letter [18], classical simulations lead to stabilization in 1D for sufficiently strong fields and sufficiently high laser frequencies. Let us start our discussion with the presentation of typical trajectories from the statistical sample. In Figs. 1 and 2 we present such trajectories that correspond to ionized electrons. Laser frequency corresponds here to "half-photon" ionization, i.e., $\omega_L = -2E \simeq 1.34$ (a.u.). The pulse shape is the same as the one used by Kulander, Schafer, and Krause [19]. Pulse duration is 105 optical periods, and turn-on and turn-off times are 5 periods. The field is chosen to be 5 a.u., so that the parameter α is $\simeq 2.55$. In these conditions ionization probability is about 0.5. After short transient the electron leaves the atom with the constant mean velocity. The second part of the motion is practically a motion of a free electron in the field. Electrons oscillate with the amplitude α, but acquire also a constant mean velocity which is determined by the pulse area acquired in the moment of detachment. Note that this velocity is not determined by a total area of the pulse, which is a unique function determined by the pulse shape. It is rather a random result of the initial part of the motion when interaction is still present.

In Figs. 3 and 4 we present analogous results for trapped electrons. Here the evidence for the Gavrila mechanism is clear. The electron undergoes two superimposed oscillations, one in the laser wave with amplitude α and period $2\pi/\omega_L$, and a much slower oscillation between the two minima of the KH potential, located at $\pm\alpha$. In another words, the electron trajectory averaged over the optical period oscillates slowly in the KH potential. The period of slow oscillation ranges between 20 (Fig. 3) and 10 (Fig. 4) optical periods.

Obviously, these properties of the trajectories exhibit themselves in the results averaged over the whole sample. In Fig. 5 we present spatial distributions of trapped and ionized electrons right after the turn on of the pulse. Here, we used a shorter (20-optical-pulse) trapezoidal pulse. Dotted lines correspond to moderate turnon and turnoff (5 periods), solid lines to a fast turnon and -off (1 period). Trapped electrons form a structure centered

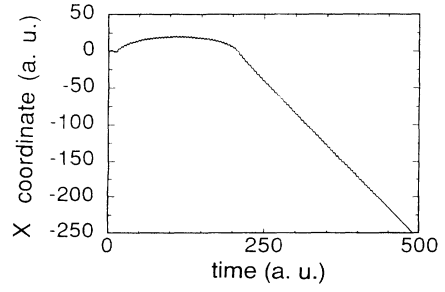

FIG. 2. Another example of a trajectory of an electron (x coordinate) ionized in the regularized 1D potential as a function of time. Parameters are the same as in Fig. 1.

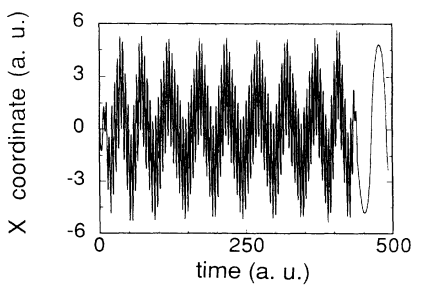

FIG. 4. Another example of a trajectory of an electron (x coordinate) trapped in the regularized 1D potential as a function of time. Parameters are the same as in Fig. 1.

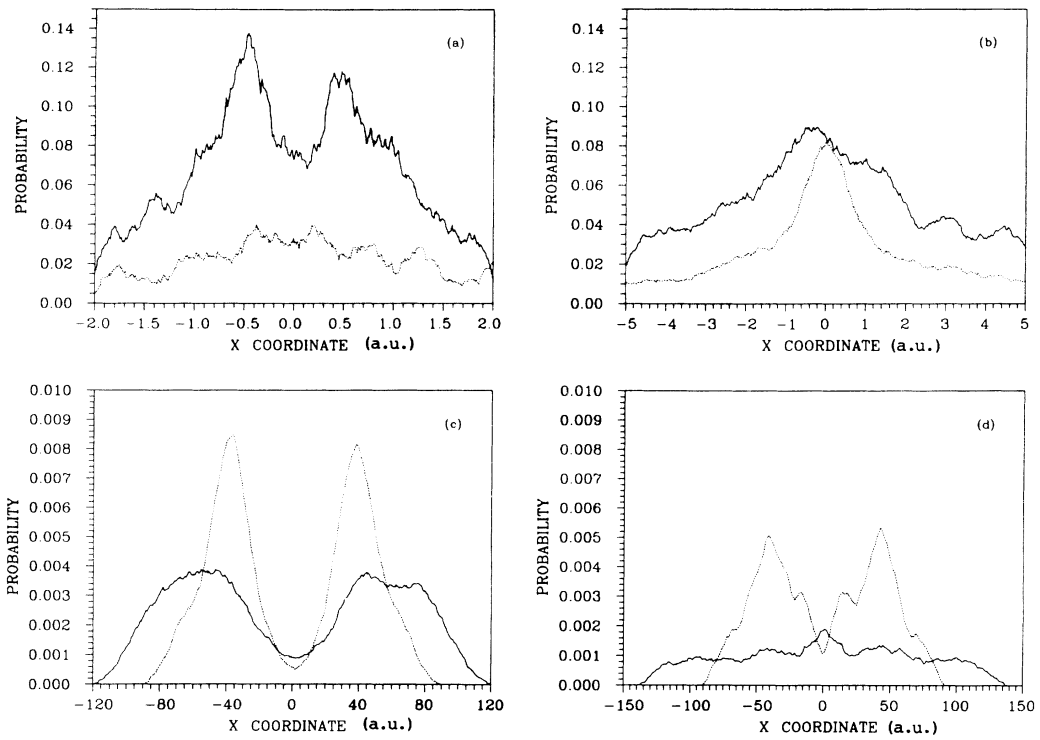

FIG. 5. (a) Spatial distributions of trapped electrons after the turn on of the laser pulse obtained with the help of a phase-space-averaging method. The laser pulse has a trapezoidal shape with $\mathcal{E}_L = 2.5$, $\omega_L = -2E$, $\omega_L T_D/2\pi = 20$. The dotted line corresponds to $\omega_L T_{\rm on}/2\pi = \omega_L T_{\rm off}/2\pi = 5$, whereas the solid line to $\omega_L T_{\rm on}/2\pi = \omega_L T_{\rm off}/2\pi = 1$. The results were averaged over the random initial phase of the laser pulse; (b) same as (a) but for $\mathcal{E}_L = 5$; (c) spatial distributions of ionized electrons after the turn on of the laser pulse obtained with the help of a phase-space-averaging method. The parameters are the same as in (a); (d) same as (c), but for $\mathcal{E}_L = 5$.

at $x = 0$ of width $\simeq \alpha$. For smaller fields [Fig. 5(a)] this structure consists of two peaks. With an increase of the field [Fig. 5(b)] this structure becomes a single, well-defined peak. Ionized electrons form two symmetric peaks far away from the nucleus. The length scale in this case is determined by the electron drift due to the acquired pulse area and pulse length. At these moderate values of $\mathcal{E}_L$, the three-peak structure predicted in Sec. II is not yet well developed. To observe it one has to increase the field to the values for which α becomes comparable to the typical distances that an electron passes due to drift effects. This is illustrated in Fig. 6, which presents distributions obtained for $\mathcal{E}_L = 50$, i.e., $\alpha = 28$. Trapped electrons form a central peak of width $\simeq \alpha$, whereas ionized electrons form two peaks located at $\pm 2\alpha$, and longer tails of the distribution. These results were

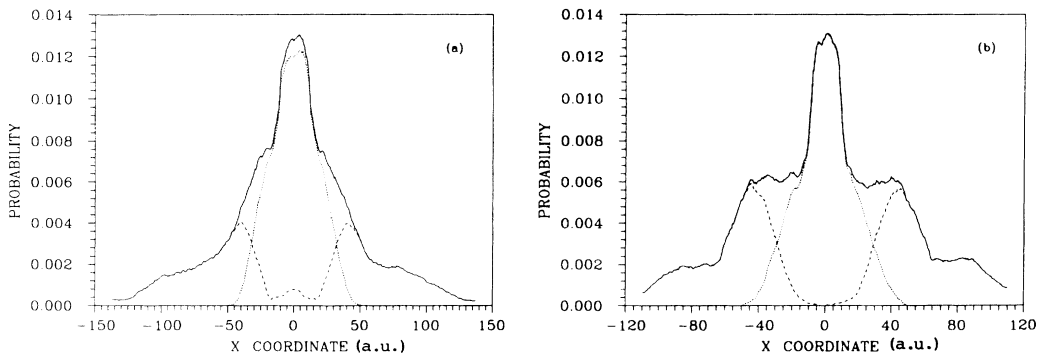

FIG. 6. (a) Spatial distributions of electrons after the turnon of the laser pulse obtained with the help of a phase-space-averaging method. The parameters are the same as in Fig 5 (a), except that $\mathcal{E}_L = 50$, and $\omega_L T_{\rm on}/2\pi = \omega_L T_{\rm off}/2\pi = 5$. The solid line represents the total distribution, the dotted line the distribution of trapped electrons, and the dashed line the distribution of ionized electrons; (b) same as (a), but for $\omega_L T_{\rm on}/2\pi = \omega_L T_{\rm off}/2\pi = 1$.

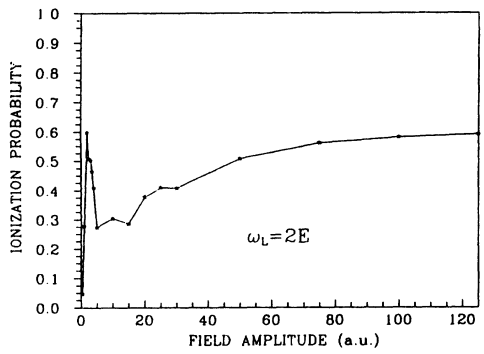

FIG. 7. Ionization probability as a function of field strength obtained from the phase-space-averaging method. The laser pulse has a trapezoidal shape with $\omega_L = -2E$, $\omega_L T_D/2\pi = 20$, and $\omega_L T_{\rm on}/2\pi = \omega_L T_{\rm off}/2\pi = 5$. Results are averaged over the initial pulse phase.

obtained after performing averaging over the uniformly distributed initial phase of the pulse.

In Figs. 7 and 8 we present results concerning total ionization probability, and its dependence on the laser frequency. The pulse shape is the same as in Figs. 5 and 6. Figure 7 was obtained for $\omega_l = 2E$. The evidence for stabilization is clear since ionization probability goes to roughly 55% as the field increases. For small field, ionization probability increases with the field in accordance with perturbation theory. Note that ionization probability has a minimum in the region when nonperturbative effects start to play a role. Here the minimum is attained already for $\mathcal{E}_L = 5$, i.e., for $\alpha \simeq 2.5$. This suggests that in classical simulation counterplay of weak-field and strong-field effects leads to optimal stabilization even before the KH potential starts to split into a developed double-well shape. We shall show in the following that it is also the case for a 3D Coulomb potential. This is a novel and unexpected feature of the classical dynamics, and we could not find any other explanation of this effect apart from the complexity of the dynamics in this region of parameters. 1D results are extremely sensitive to frequency increase. The structure shown in Fig. 7 can still be seen in Fig. 8 obtained for $\omega_L = 2.8E$, but the total ionization is here strongly suppressed. This suppression

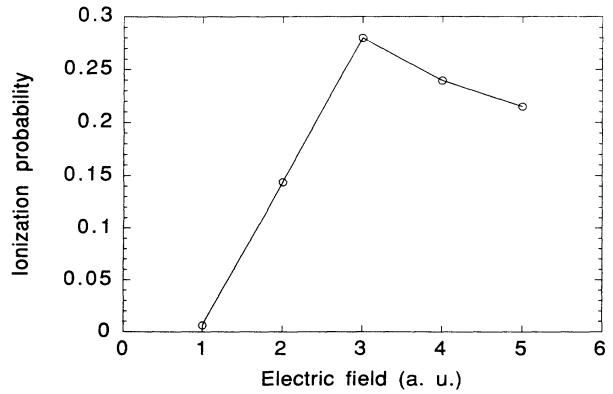

FIG. 8. Same as Fig. 7, but for $\omega_L = -2.8E$.

is connected with the fact that the increase of the frequency means practically that we enter the weak-field regime. Nevertheless, the optimal stabilization (minimal ionization probability) shifts towards smaller values of α. For even larger values of $\omega_L \geq 3E$ the ionization probability is practically zero for $\alpha \leq 1$ and becomes finite $\simeq 50\%$ when α becomes larger than 1. The interesting structure discussed above cannot be well resolved in this case. This is, however, in accordance with our Fig. 3 from Ref. [18], which shows that a rapid decrease of ionization probability with the increase of the "effective" photon number.

Our results indicate that for ionized electrons the acquired drift plays an essential role. Such drift may be acquired already in the initial part of the motion provided the turn-on time $T_{\rm on}$ is very short. We observed indeed the dependence of ionization probability on $T_{\rm on}$. For smaller values of $\omega_L \leq 3$, there is an optimal turnon time being equal to several optical periods. Adiabatic turn-on leads to rather effective weak-field ionization. For $\omega_L = 2E$ the stabilization mechanism is still quite effective for $T_{\rm on}$ equal to 1 period, but it apparently breaks down for $T_{\rm on} = 0$. In the latter case one could expect that the pulse $\mathcal{E}_L \Theta(t) \sin \omega_L t$ should lead to a stronger ionization than $\mathcal{E}_L \Theta(t) \cos \omega_L t$ where $\Theta(t)$ is the Heaviside function. The reason is that for free electrons the first one leads to maximal drift, whereas the second does not introduce any drift effects at all. In reality, the situation is more complex, since the interaction with the potential plays a role in the initial part of the motion and the total resulting drift is a combined effect of free-electron motion and the action of the potential forces. For $\omega_L = -2E$, $\mathcal{E}_L = 5$, and $T_{\rm on} = 0$ we have observed practically 100% ionization, but we have also seen very strong correlations between the final energies of the electrons and the initial phase of the laser pulse. There are optimal choices of this phase that lead to minimal ionization probability, or at least to very small positive values of the final electronic energy. The value of such an optimal phase cannot be guessed easily as it results from complex interaction in the initial part of the dynamics.

We stress again that the above results agree very well with the results of the exact quantum-mechanical analysis (see also [28]). For the smoothed one-dimensional potentials this fact has been for the first time observed by Dando and Richards [21]. We turn now to the discussion of the 3D result, and show essentially different features of the classical dynamics in that case.

V. LACK OF STABILIZATION IN THE 3D COULOMB POTENTIAL

In this section we present results concerning classical simulations for the 3D Coulomb potential. Generally speaking, in this case stabilization can hardly be seen, unless one uses unrealistically high values of laser frequencies [18]. For realistic frequencies (say "half-photon" ionization) ionization probability very quickly attains values close to 1 when the field increases and α becomes of the order of one. The physical reason is the following: electrons are strongly bounded initially and may be subject

to very strong Coulomb forces in the initial part of the motion. They absorb then a large portion of energy and angular momentum, and due to the fact that the phase space is larger in 3D than in 1D they immediately leave the vicinity of the nucleus. Even if some electrons remain trapped after the pulse turnoff, the mechanism of trapping has nothing to do with the Gavrila mechanism. After initial transient, electrons may land on highly excited Rydberg orbits, which are well separated from the potential center. Electrons on such orbits feel very weak Coulomb forces, and practically do not absorb energy in the field on average, just like free electrons in the field. These statements are very general in nature, and do not depend practically on the pulse parameters (pulse shape, field strength, frequency, duration times, turnon and turnoff, drift effects, etc.) They also depend very weakly on the properties of the initial state (form of an ensemble, initial energy and angular momentum, etc.). We illustrate these results below.

Let us first discuss the dependence on the pulse shape. In our Letter we discussed results for short trapezoidal pulses (T_D equal to 20 optical periods). Figure 9 contains results for an adiabatically turned on sinusoidal and longer (105 optical pulses) pulse. Here again $\omega_L = -2E$, but $E = -\frac{1}{2}$ for 3D hydrogen. Ionization probability is close to 98%. Note the small structure for $\mathcal{E}_L \simeq 5$ (i.e., $\alpha = 5$). This is the same structure as observed in 1D. It results from the interplay of perturbative and nonperturbative character of the motion, and as we shall see below is not directly connected to the Gavrila mechanism. We have also made simulations for rapidly turned on pulses, as well as checked the sensitivity of the results with respect to the initial pulse phase. Figure 9 was obtained after performing an average over this phase, but the results obtained with fixed phase are quite analogous. No significant correlation between the initial phase and ionization probability has been observed.

A similar conclusion follows from Fig. 10, which presents the dependence of the ionization probability on initial angular momentum. In the simulations we have used various initial ensembles corresponding to different values of the angular momentum. For $E = -\frac{1}{2}$, L may range between 0 and 1, corresponding to a different eccentricity of electrons. In Fig. 10 we show the results for limiting cases $L = 0$ and $L = 1$, and short laser pulse with T_D equal to 20 optical periods. All the other results for intermediate L lie between the two displayed curves. The ionization probability for moderate field ($\mathcal{E}_L = 2$) can be quite reduced for ensembles with large L. This can be understood in classical terms, since for $L = 1$ the ensemble consists of electrons on circular orbits. Such electrons feel weaker potential forces and have less chance to absorb energy in the field. Quantum mechanically this corresponds to the fact that corresponding dipole transition matrix elements are larger for $L = 0$ than for $L = 1$. In Fig. 10(a) we show that with decreasing effective photon number ($n_{\rm ph} = -E/\omega_L$) or, in other words, with increasing laser frequency ionization probability falls down

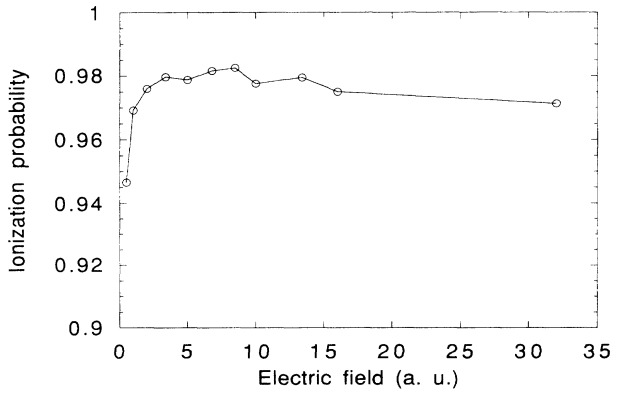

FIG. 9. Ionization probability as a function of field strength for the 3D Coulomb potential. The laser pulse has a sinusoidal shape with $\omega_L = -2E$, $\omega_L T_D/2\pi = 105$, and $\omega_L T_{\rm on}/2\pi = \omega_L T_{\rm off}/2\pi = 30$. Results are averaged over the initial pulse phase.

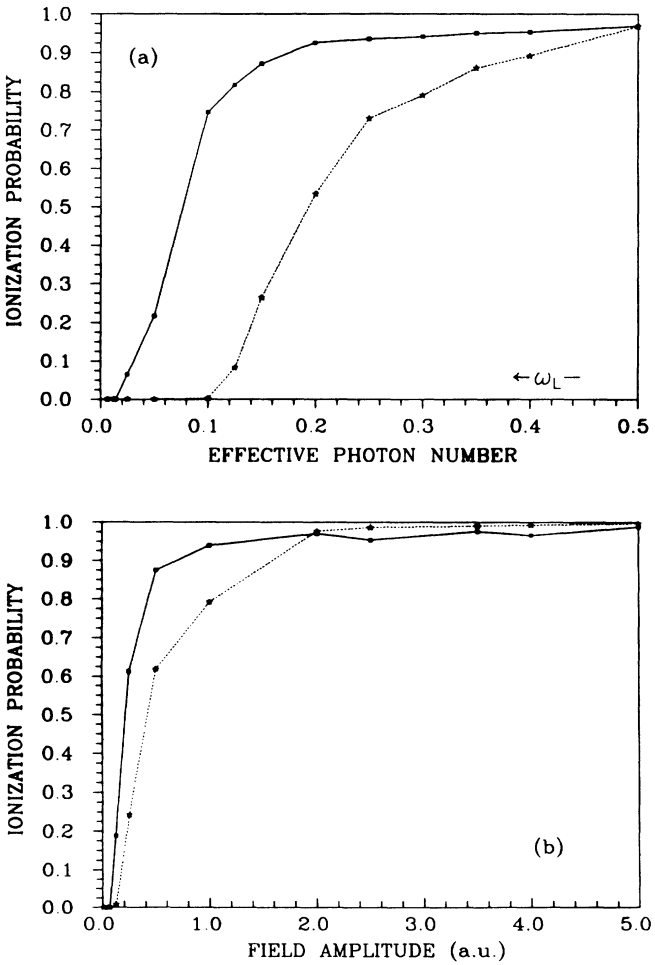

FIG. 10. (a) Ionization probability as a function of effective photon number, $n_{\rm ph} = -E/\omega_L$, for the 3D Coulomb potential. The laser pulse has a trapezoidal shape with $\omega_L = -2E$, $\omega_L T_D/2\pi = 20$, and $\omega_L T_{\rm on}/2\pi = \omega_L T_{\rm off}/2\pi = 5$. Results are averaged over the initial pulse phase. The dotted line corresponds to initial angular momentum $L = 1$, the solid line to $L = 0$. (b) Same as (a), but displayed as a function of the field strength for the fixed $\omega_L = -2E$.

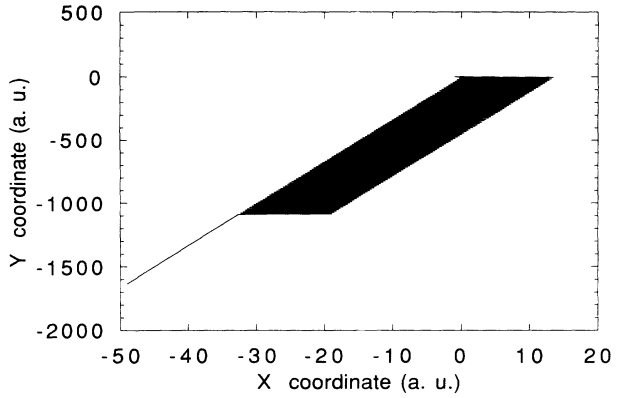

FIG. 11. Trajectory of an electron (x and y coordinates) ionized in the 3D Coulomb potential. The laser pulse has a sinusoidal shape with $\mathcal{E}_L = 6.8$, $\omega_L = -2E$, $\omega_L T_{\rm on}/2\pi = 5$, $\omega_L T_D/2\pi = 105$, and $\omega_L T_{\rm off}/2\pi = 5$. The initial phase of the pulse has been chosen randomly.

to zero for $\omega_L \simeq 5$ for $L = 1$, and for $\omega_L \simeq 40$–50 for $L = 0$. Note, however, that for "half-photon" ionization ($\omega_L = 1$), both curves practically coincide. This is even more evident in Fig. 10(b) where we display ionization probability as function of the field strength for $\omega_L = -2E = 1$. Although for weak field the ionization degree for $L = 1$ is smaller, both curves very quickly saturate on the level close to 1 for field strengths larger than 2 a.u. Even more, our results suggest that ionization probability for $L = 1$ becomes systematically larger than that for $L = 0$ for such strong fields. This can be understood, since for strong fields the forces induced by the laser can easily push electrons toward the potential center where Coulomb forces are extremely large. Electrons acquire then both energy and angular momentum. Those that initially had already momentum may acquire even more, and therefore may more easily explore large regions of the phase space in order to escape.

Gavrila and Burnett [26] suggested recently that the best initial state for achieving stabilization would be a state of maximal angular momentum, with maximal projection of this momentum on the polarization axis, x. In classical terms such a state corresponds to a circular orbit

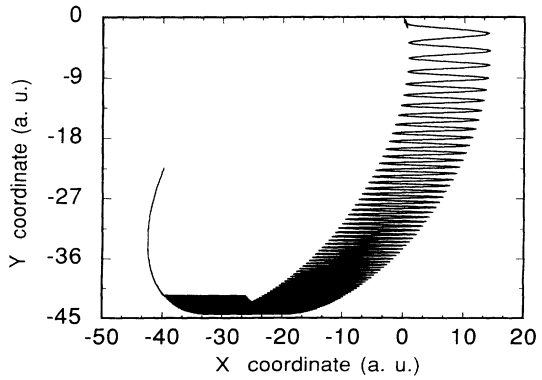

FIG. 12. Trajectory of an electron (x and y coordinates) trapped in the 3D Coulomb potential. Parameters are the same as in Fig. 11.

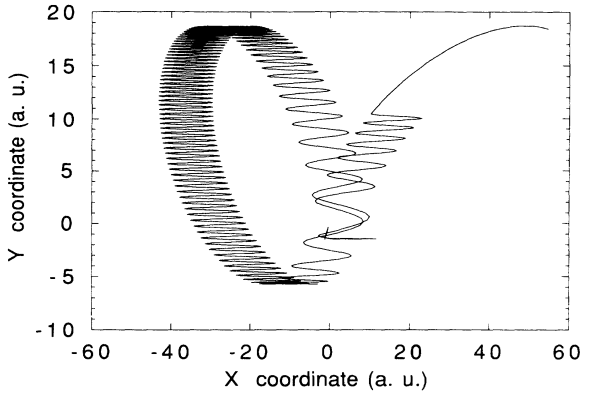

FIG. 13. Another example of a trajectory of an electron (x and y coordinates) trapped in the 3D Coulomb potential. Parameters are the same as in Fig. 11.

in the y-z plane . We have checked that the ionization is not suppressed when such initial state is used in classical simulations.

The lack of stabilization in the discussed regime of parameters in the 3D Coulomb potential suggests that the Gavrila mechanism does not work here at all. Indeed, a closer look on typical trajectories shows this directly. In Figs. 11–13 we present typical trajectories for ionized and bound electrons. In both cases the electron gains energy on the mean during the very initial part of its motion (first, or couple of first periods). It ends up then in an ionized state that corresponds to an escape with constant velocity (Fig. 11), or in a highly excited Rydberg state (Fig. 12). For such a state the electron is mostly far from the nucleus and in the mean sense does not practically absorb energy anymore. Generic trajectories of trapped electrons have this one-step character. Figure 13 shows a rare example of a two-step process. The electron lands in a first step in a moderately high Rydberg state, enters the vicinity of nucleus, absorbs energy once more, and finally ends up in an even higher Rydberg state. Obviously, the final spatial distribution is determined by length scales that do not have anything in common with α. Distribution of ionized electrons is characterized by typical acquired drift (which depends on the energy gain in the initial phase and on the duration of the remaining part of the pulse). Distribution of trapped electrons is characterized by a typical size of final Rydberg states.

The fact that electrons typically absorb energy during the first couple of periods can be expressed in statistical terms. To this aim we calculate reduced absorbed energy (see also Richards [22]), as

$$\langle E_{\rm red}(t)\rangle = \langle E(t)\rangle - \langle v^2_{\rm quiv}(t)/2\rangle, \tag{20}$$

where $\langle\,\rangle$ denotes both the sample average and the time average over one optical cycle $[t_1, t_1+2\pi/\omega_L]$. The second term on the right-hand side has a physical meaning of the quiver energy during this cycle, with velocity defined as

$$v_{\rm quiv}(t) = \int_{t_1}^{t} \mathcal{E}_L f(t)\cos(\omega_L t + \phi). \tag{21}$$

Such a definition assures that absorption of reduced en-

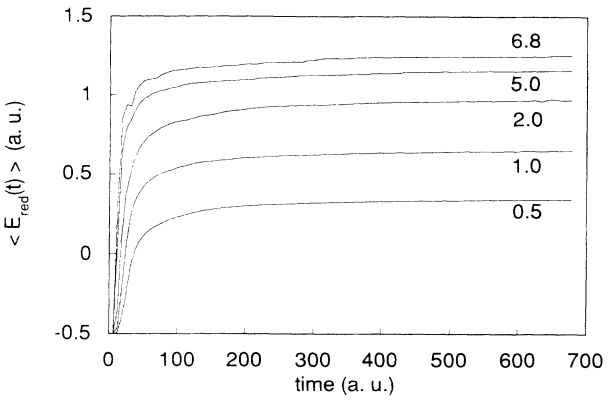

FIG. 14. Reduced energy as a function of time for indicated values of the field strength. Other parameters of the laser pulse are the same as in Fig. 11.

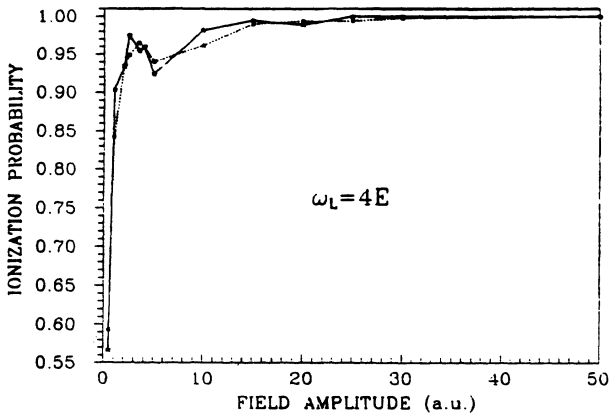

FIG. 16. Ionization probability as a function of the field strength for $\omega_L = -4E$. Other parameters of the laser pulse are the same as in Fig. 10(a).

ergy follows a smooth curve. In Fig. 14 we present $\langle E_{\rm red}(t)\rangle$ for indicated values of the field strength. Absorption, as we see, takes place for $t \leq 35$, i.e., $t \leq 5$ optical periods. After, the transient electron enters a plateau region, where energy increases very slowly. Note that the level of the plateau increases with increasing $\mathcal{E}_L$.

There are, however, signatures of stabilization, i.e., reduction of ionization probability or photoabsorption rate in our data. Although they do not correspond directly to the Gavrila mechanism, they are worth mentioning. First of all, the mean rate of energy absorption in the plateau region,

$$\gamma = \frac{1}{\langle E_{\rm red}(t)\rangle}\frac{\Delta\langle E_{\rm red}(t)\rangle}{\Delta t}, \tag{22}$$

is a decreasing function of the field strength (Fig. 15). This expresses the fact that with the increase of $\mathcal{E}_L$ both ionized and trapped electrons are further from the nucleus. The weaker the interaction, the smaller is the absorption rate. Note, however, that the rates in Fig. 15 are an order of magnitude smaller from those calculated in the quantum theory of Kulander, Schafer, and Krause [19].

Other signatures of stabilization are shown in Figs. 16 and 17. We show here ionization probability as a function of the field strength for different values of ω_L. Although ionization very quickly becomes total, we observe a characteristic minimum in the curves that reflects complex interplay between weak- and strong-field effects. Note that as in 1D case the minimum occurs for $\alpha < 1$ for large enough ω_L (i.e., $\alpha \simeq 0.3$ in Fig. 17). This indicates that the physical origins of this effect cannot be explained by the Gavrila mechanism. Recently, Shakeshaft [39] introduced another criterion for stabilization. According to this argument, stabilization should occur when the quiver energy is comparable to the energy of a single photon. Note that the characteristic field strength in this case is typically smaller than if $\alpha \geq 1$.

Summarizing, we would like to stress the distinction between the two discussed mechanisms of ionization suppression. The first one (A) employs the fact that *a free electron on average does not absorb energy.* A bounded electron, thus, can only gain energy from a laser pulse close to the nucleus, i.e., during *scattering on the Coulomb potential.* The second one (B) is the mecha-

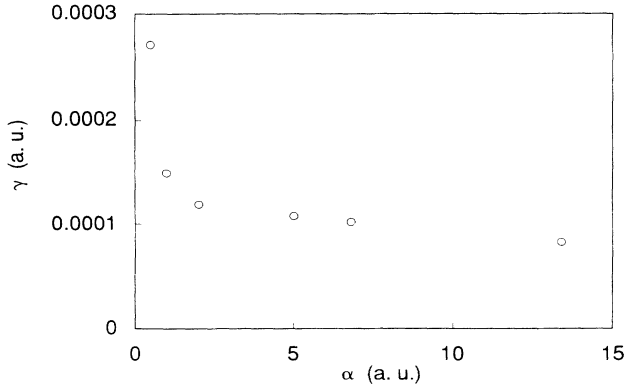

FIG. 15. Mean rate of energy absorption in the plateau region (see Fig. 14) as a function of the field strength. Parameters of the laser pulse are the same as in Fig. 11.

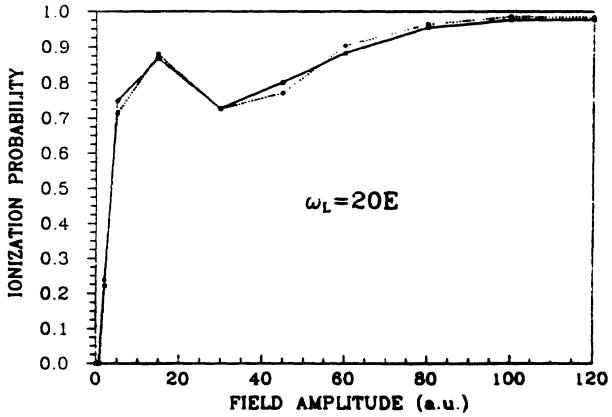

FIG. 17. Same as in Fig. 16, but for $\omega_L = -20E$.

nism of Gavrila and co-workers, described in our recent Letter [18] and in this paper. According to this mechanism, an electron is caught in the effective double-well potential in the Kramers-Henneberger (KH) frame of reference. Of course in reality both mechanisms contribute to the complex dynamics of electrons.

Mechanism A explains very well the suppression of ionization with increasing frequency of the laser, when both pulse intensity and the number of cycles are kept constant (compare Fig. 3 in Ref. [18]). It predicts suppression of ionization for less-eccentric orbits. In particular, it suggests weaker ionization in 3D (where fewer orbits are eccentric) than in 1D (where all orbits are eccentric). This mechanism does not explain well the main feature of the so-called *stabilization of atoms*, i.e., decreasing ionization probability with increasing laser intensity. This mechanism works well in the regime of small α.

Our recent Letter and this paper are mainly devoted to the study of mechanism B, i.e., the Gavrila mechanism. In the KH frame the electron moves in an effective potential V_{eff}. For large α this potential has two minima. If the electron has negative energy in the KH frame, with probability $\simeq \frac{1}{2}$ it will remain bounded in the lab frame. This mechanism works well for high frequencies, since only then are the corrections to V_{eff} small.

Contrary to mechanism A, mechanism B works better for larger α. Mechanism B, as well as the notion of V_{eff}, is more efficient for more eccentric orbits, provided the forces that the electron fell close to the potential center are not too large. In particular, it works strongly in 1D regularized potentials. For a given initial configuration it is sensitive to the switch-on of the pulse.

In Ref. [18] we considered short and rapidly switched-on pulses that are accessible in experiments. We attempted to answer a fundamental question: Is it possible to introduce the electron into the negative energy orbit in the KH frame? Our simulations show that it is hardly possible in the 3D Coulomb potential. For such short pulses the electron rapidly changes its energy and angular momentum during the switch-on, when it remains close to the nucleus. Our simulations show that second encounters with the nucleus are very rare. After the switch-on the electron is practically free, and its energy gain is very slow. In this phase, mechanism A plays a role, and the energy gain rate is the decreasing function of the laser intensity.

In the 1D smoothed potential the electron passes the nucleus in every cycle and may equally well gain or loose energy. These energy changes, however, are bounded, since such are the forces acting on the electron in the regularized potential (see also [21]). In the KH frame a large fraction of electrons might have negative energies, and the electronic distribution in the lab frame has indeed a characteristic three-peaked shape. We stress the following:

(1) There is a very good quantitative agreement [28] for small principal quantum numbers n between quantum and classical dynamics of the 1D model of Eberly and co-workers [27].

(2) Those results and experience with the 1D model suggest that for large $n \gg 1$ and small l, and in the regime of large α, the quantum and classical systems will behave similarly in 3D.

(3) On the other hand, the results of quantum calculations in 3D from the ground state predict much weaker ionization [19] than the classical theory. We attribute this discrepancy to the differences accumulated during the switch-on of the laser pulse, when the electric field grows from weak to strong values.

The following question arises: What is the physical reason of the above-mentioned discrepancy? To answer this we looked for conditions under which stabilization according to mechanism B can be observed in the 3D system.

VI. STABILIZATION IN THE 3D REGULARIZED POTENTIAL

As we have shown, the lack of stabilization in the 3D Coulomb potential is due to a large energy gain in the initial phase of the motion. In this transient the electron feels large Coulomb forces that cannot be overcome by the laser field. It is natural to expect that the situation is different, when we impose bounds on the potential forces by regularizing the potential.

We have performed simulations in the 3D regularized potential of the form

$$V(r) = 1/(r + \epsilon). \tag{23}$$

Our results show that indeed, independently of the form of regularization (23) (and to great extent independently of the initial energy and angular momentum, etc.) stabilization according to mechanism B will occur and will dominate laser-atom interactions, provided regularization length ϵ is of the order of 1. The results obtained with such ϵ compare much better to the quantum-mechanical results obtained for the pure Coulomb case. One may say that the principal effect of quantum mechanics is regularization of Coulomb singularity due to

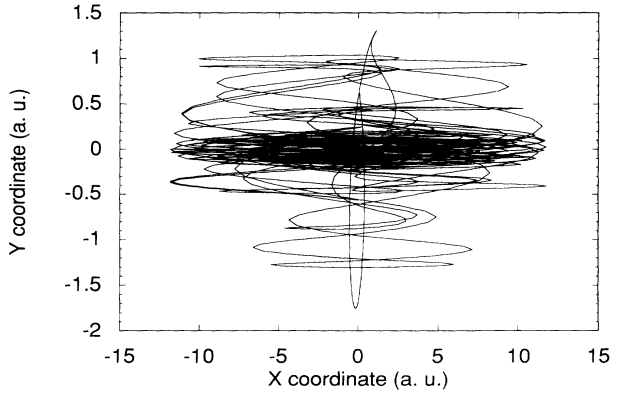

FIG. 18. Trajectory of an electron (x and y coordinates) trapped in the 3D regularized potential with $\epsilon = 2$. The laser pulse has a sinusoidal shape with $\mathcal{E}_L = 6$, $\omega_L = -2E$, $\omega_L T_{\text{on}}/2\pi = 5$, $\omega_L T_D/2\pi = 105$, and $\omega_L T_{\text{off}}/2\pi = 5$. The initial phase of the pulse has been chosen randomly.

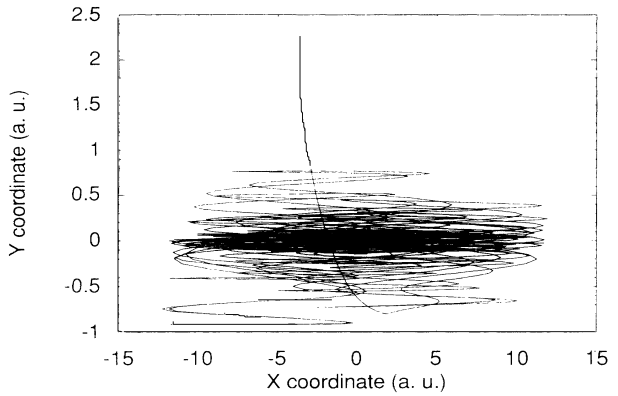

FIG. 19. Another trajectory of an electron (x and y coordinates) trapped in the 3D regularized potential for $\epsilon = 2$. Parameters are the same as in Fig. 18.

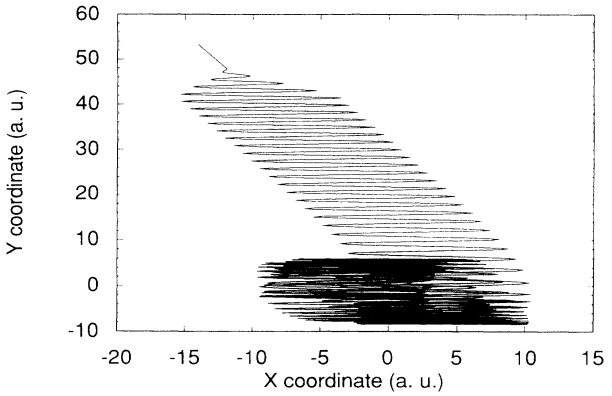

FIG. 21. Trajectory of an electron (x and y coordinates) trapped in the 3D regularized potential with $\epsilon = 1$. Other parameters are the same as in Fig. 18.

quantum uncertainty. In Figs. 18 and 19 we show typical trajectories obtained for $\epsilon = 2$. For such cases most electrons remain trapped. Figure 18 shows clear evidence for mechanism B of Gavrila. Electronic motion consists of three superimposed oscillations:

- "free" oscillations of the x coordinate in the field with amplitude α;
- slower oscillations of the x coordinate between the minima of the KH potential located at $\pm 2\alpha$;
- item oscillations in the transverse direction (y or z) characterized by a much smaller amplitude.

Note that the latter has a quasichaotic character (Fig. 18). Sometimes (but very rarely) the motion of the trapped electron has a very regular character leading to Lissajou-like curves. Such periodic orbits extend from $-\alpha$ to α in the x direction. They occur more frequently for other smoothed potentials, i.e., for potentials with a repulsive core at $r = 0$.

In Figs. 20–22 we present results for the intermediate case $\epsilon = 1$. Here the ionization degree is roughly 50% and compares well with the quantum-mechanical results of Kulander. Ionized trajectories display similar character as in the Coulomb case (Fig. 20). After some transient, electrons leave the nucleus with constant mean velocity. Trapping of electrons occurs as a joint result of two mechanisms (A and B). They may bounce for some time in the KH potential (mechanism B). Since in this motion they pass sometimes close to the nucleus, they may sometimes absorb enough energy to jump to a highly excited Rydberg state. There the electrons are typically far from the nucleus and are stabilized according to the mechanism A. The trapping may have a one-step character (from KH potential to Rydberg orbit; see Fig. 21) or a multistep character (KH → Rydberg → KH → Rydberg → etc.; see Fig. 22).

In Fig. 23 we show ionization probability as a function of the field strength. The evidence of stabilization is obvious. Note that this result compares much better with quantum-mechanical results of Kulander than any of the curves obtained for the pure Coulomb potential.

From the analysis of trajectories it follows that an electron trapped in the KH potential will have a tendency to escape in the transverse direction (both in order to ionize, as well as in order to become trapped in one of the

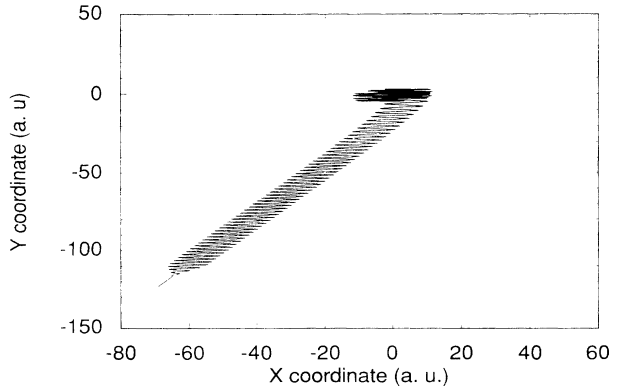

FIG. 20. Trajectory of an electron (x and y coordinates) ionized in the 3D regularized potential with $\epsilon = 1$. Other parameters are the same as in Fig. 18.

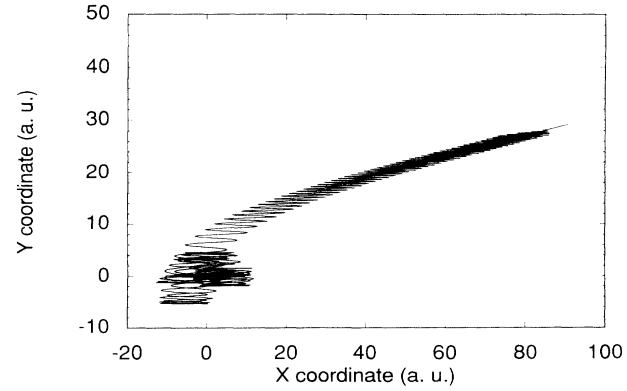

FIG. 22. Another trajectory of an electron (x and y coordinates) trapped in the 3D regularized potential with $\epsilon = 1$. Other parameters are the same as in Fig. 18.

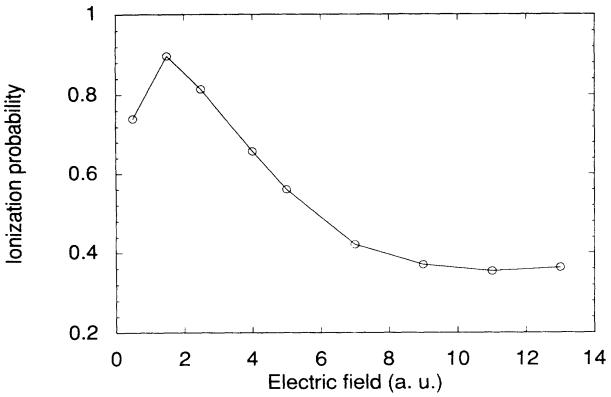

FIG. 23. Ionization probability as a function of the field strength for the 3D regularized potential with $\epsilon = 1$. Other parameters are the same as in Fig. 18.

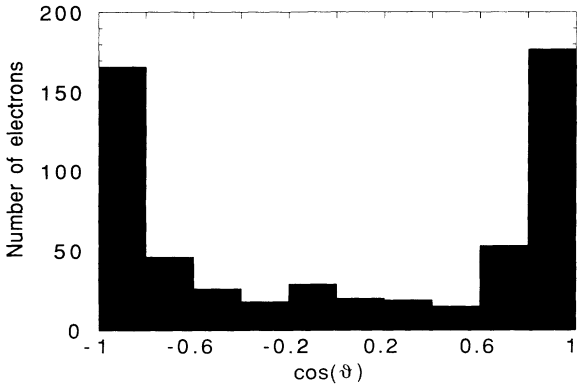

FIG. 25. Angular distribution of ionized electrons for the case of a regularized potential with $\epsilon = 1$. The parameters of the pulse are the same as in Fig. 18, except $\mathcal{E}_L = 2$.

Rydberg states). Angular distribution of electrons should therefore be more concentrated for angles $\theta = \pi/2$, where θ denotes the angle between the final electron velocity and polarization axis x.

This should be in contrast with: (a) the results for weak fields, where escape should rather take place in the direction of polarization; (b) the results for the pure Coulomb case. We illustrate this point in Figs. 24–26. Indeed, angular distributions for regularized potential are more pronounced for $\theta = \pi/2$ for large fields. For weak fields (Fig. 25) and for the pure Coulomb case (Fig. 26) ionization occurs mainly along the polarization axis. Note that contrary to Fig. 24, the distribution in Fig. 26 is not symmetric and is in fact sensitive to the initial phase of the laser pulse.

VII. CONCLUSIONS

We have presented a detailed classical theory of stabilization of atoms in very strong laser fields. We have shown that two mechanism of ionization suppression are relevant for the dynamics: (A) lack of absorption for quasi-free-electrons; (B) trapping in the KH potential. Our main results may be summarized as follows:

- For pure Coulomb potential trapping in the KH potential in the statistical sense is hardly possible. If, however, electrons are trapped, this occurs due to mechanism A. They land on highly excited Rydberg orbits.
- For regularized potentials (both in 3D and 1D) stabilization according to mechanism B is very efficient. Motion of trapped electrons is quasi-one-dimensional.
- Classical dynamics predicts minima of ionization probability for $\alpha < 1$ for both Coulomb and regularized potentials. This is a novel effect, and it is not clear how to relate it to mechanism A or B.
- The results for regularized potentials in 3D agree with quantum-mechanical results obtained for the Coulomb potential [19]. We speculate that the major quantum-mechanical effect in the process of ionization by ultrastrong, high-frequency pulses consists in smoothing of the Coulomb singularity. On the other hand, one should stress that the results of quantum-mechanical calculations of Kulander, Schafer, and Krause [19] corre-

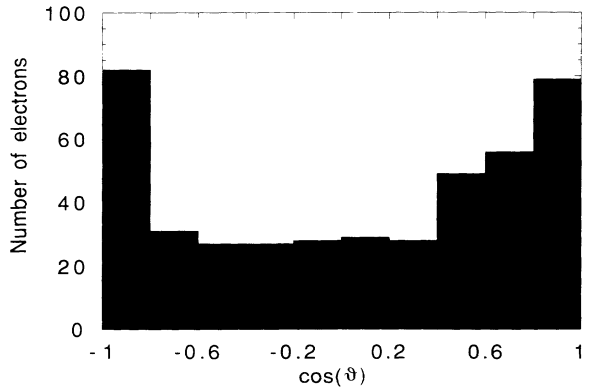

FIG. 24. Angular distribution of ionized electrons for the case of regularized potential with $\epsilon = 1$. We present the number of electrons as a function of the cosine of the angle between the final velocity and polarization axis. The parameters of the pulse are the same as in Fig. 18.

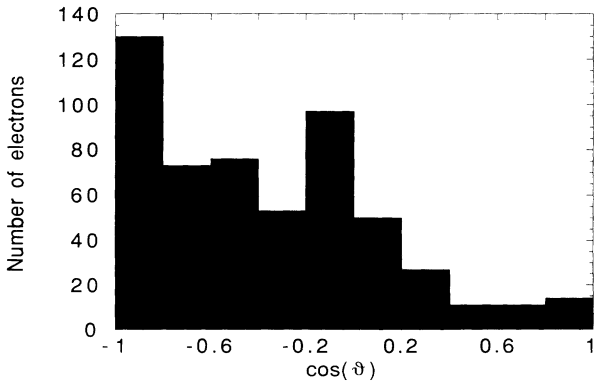

FIG. 26. Angular distribution of ionized electrons for the case of Coulomb potential. The parameters of the pulse are the same as in Fig. 18.

spond effectively to a smoothed potential. This is due to a finite grid of the order of 0.15 a.u. used in the numerical method (see [40]). From this point of view the results of Kulander, Schafer, and Krause should be compared with the results of classical analysis for regularized potentials.

We stress that we do not claim that the results of Kulander, Schafer, and Krause are due to a finite grid, and that the existence of stabilization is questionable. We would like only to point out the importance of potential smoothing. In our opinion it would be very interesting to compare quantum-mechanical results for pure Coulomb and smoothed potentials in the discussed regime of parameters.

Note that the situation that we discuss cannot be directly compared with that described in Gavrila's calculations that lead to trapping. The reason is that we fully account for the effects of the pulse turnon and turnoff. According to classical theory, it is exactly during the turnon, when the electron attains very large accelerations and ionize in the Coulomb potential.

ACKNOWLEDGMENTS

M.L. acknowledges the support of the KBN Grant "Quantum Chaos." We acknowledge fruitful discussions with K. Burnett, J. H. Eberly, R. Grobe, M. Yu. Ivanov, B. Piraux, L. Roso-Franco, P. L. Knight, K. C. Kulander, J. Mostowski, and Q. Su.

* Institute of Physics, Polish Academy of Sciences, 02-668 Warsaw, Poland.

[1] L. I. Schiff, *Quantum Mechanics* (McGraw-Hill, New York, 1968).

[2] F. Haake, *Quantum Signatures of Chaos* (Springer, Heidelberg, 1991).

[3] See, for instance, G. Casati, B. V. Chirikov, D. L. Shepelyansky, and I. Guarneri, Phys. Rep. **154**, 77 (1987).

[4] G. Casati, B. V. Chirikov, and D. L. Shepelyansky, Phys. Rev. Lett. **63**, 2525 (1984); J. G. Leopold and D. Richards, J. Phys. B **21**, 2179 (1988).

[5] J. E. Bayfield, in *Quantum Measurement and Chaos*, edited by E. R. Pike and S. Sarkar (Plenum, New York, 1987), and references therein.

[6] J. G. Leopold and I. C. Percival, Phys. Rev. Lett. **41**, 944 (1978); J. Phys. B **12**, 709 (1979).

[7] I. C. Percival, in *Advances in Chemical Physics*, edited by I. Prigogine and S. A. Rice (Wiley, New York, 1977), Vol. XXXVI.

[8] J. Mostowski and K. Życzkowski, Z. Phys. D **5**, 293 (1987).

[9] G. A. Kyrala, J. Opt. Soc. Am. B **4**, 731 (1987).

[10] J. Grochmalicki, J. Mostowski, and M. Trippenbach, J. Phys. B **21**, 1673 (1988); J. Grochmalicki, M. Lewenstein, M. Wilkens, and K. Rzążewski, J. Opt. Soc. Am. B **7**, 607 (1990).

[11] J. Javanainen, J. H. Eberly, and K. Rzążewski, Phys. Rep. **204** (5), 331 (1991).

[12] G. Bandarage, A. Maquet, and J. Cooper, Phys. Rev. A **41**, 1744 (1990).

[13] For the earliest reference, see I. Gersten and M. H. Mittleman, J. Phys. B **9**, 2561 (1976).

[14] M. Gavrila and J. Z. Kamiński, Phys. Rev. Lett. **52**, 613 (1984); M. Pont, N. R. Walet, M. Gavrila, and C. W. McCurdy, *ibid.* **61**, 939 (1988); M. Gavrila, *Conference on Super-Intense Laser Atom Physics, Abstracts*, edited by J. H. Eberly and W. G. Greenwood (University of Rochester, Rochester, NY, 1989).

[15] Q. Su, J. H. Eberly, and J. Javanainen, Phys. Rev. Lett. **64**, 862 (1990); Q. Su and J. H. Eberly, J. Opt. Soc. Am. B **7**, 564 (1990).

[16] V. C. Reed, P. L. Knight, and K. Burnett, Phys. Rev. Lett. **67**, 1415 (1991).

[17] H. A. Kramers, in *Les Particules Elementaires*, Proceedings of the Eighth Solvay Conference, edited by R. Stoops (Wiley, New York, 1950); W. C. Henneberger, Phys. Rev. Lett. **21**, 838 (1964); C. K. Choi, W. C. Henneberger, and F. C. Sanders, Phys. Rev. A **9**, 1895 (1974); see also P. L. Kapitza, Zh. Eksp. Teor. Fiz. **21**, 588 (1951); Y. Pomeau, Ann. Inst. Henri Poincaré **45**, 29 (1986).

[18] J. Grochmalicki, M. Lewenstein, and K. Rzążewski, Phys. Rev. Lett. **66**, 1038 (1991).

[19] K. C. Kulander, K. J. Schafer, and J. L Krause, Phys. Rev. Lett. **66**, 2601 (1991); see also K. C. Kulander, K. J. Schafer, and J. L Krause, in *Multiphoton Processes*, edited by G. Mainfray and P. Agostini (CEA, Paris, 1991).

[20] L. You, J. Mostowski, and J. Cooper, Phys. Rev. A **45**, 3203 (1992).

[21] The differences between Coulomb and smoother potentials have been discussed earlier, see P. A. Dando and D. Richards, J. Phys. B **23**, 3179 (1990), and references therein.

[22] D. Richards, in *Aspects of Electron-Molecule Scattering and Photoionization*, edited by A. Herzenberg, AIP Conference Proceedings (American Institute of Physics, New York, 1990); J. G. Leopold and D. Richards, J. Phys. B **22**, 1931 (1989).

[23] L. D. Landau and E. M. Lifshitz, *Mechanics* (Addison-Wesley, Reading, MA, 1960).

[24] Technical Digest, II Conference on Super Intense Laser-Atom Physics, SILAP '91, Big Sky, Montana (unpublished).

[25] P. Lambropoulos, Phys. Rev. Lett. **35**, 2141 (1985).

[26] See contributions of M. Gavrila and K. Burnett to Ref. [24].

[27] J. Javanainen, J. H. Eberly, and Q. Su, Phys. Rev. A **38**, 3430 (1988); J. H. Eberly, Q. Su, and J. Javanainen, J. Opt. Soc. Am. B **6**, 1289 (1989).

[28] R. Grobe and C. K. Law, Phys. Rev. **44**, 4114 (1991).

[29] J. Mostowski, Acta Phys. Polon. A **56** (1979); J. Mostowski and J. J. Sanchez-Mondragon, Opt. Commun. **3**, 293 (1979).

[30] J. Parker and C. R. Stroud, Jr., Phys. Rev. Lett. **56**, 716 (1986); J. A. Yeazell and C. R. Stroud, Jr., *ibid.* **60**, 716 (1988).

[31] V. I. Arnold, *Mathematical Methods of Classical Mechanics* (Springer-Verlag, Berlin, 1978).

[32] C. W. Gardiner, *Handbook of Stochastic Methods for Physics, Chemistry, and the Natural Sciences* (Springer-

Verlag, Berlin, 1983).
[33] K. Takahashi, Progr. Theor. Phys. (Suppl.) **98**, 109 (1989).
[34] E. Wigner, Phys. Rev. **40**, 749 (1932).
[35] R. J. Glauber, Phys. Rev. **131**, 2766 (1963).
[36] K. Husimi, Proc. Phys. Math. Soc. Jpn. **22**, 264 (1940).
[37] J. Mostowski has performed extensive studies of possible applications of various quasiprobabilities in this context (private communication).
[38] Recently, L. Roso-Franco observed that the "Rochester" 1D potential may be derived from the 3D Coulomb potential, provided one uses cylindrical coordinates so that the z axis is a polarization axis. One then has to "freeze" the ρ variable at its initial quantum-mechanical mean value.
[39] R. Shakeshaft, in Ref. [24].
[40] K. C. Kulander, Phys. Rev. A **35**, 445 (1987).

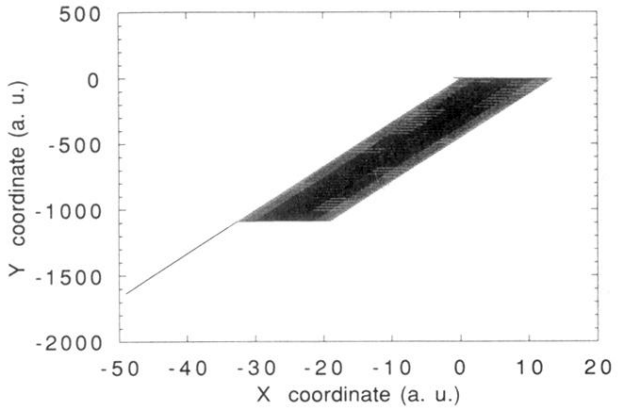

FIG. 11. Trajectory of an electron (x and y coordinates) ionized in the 3D Coulomb potential. The laser pulse has a sinusoidal shape with $\mathcal{E}_L = 6.8$, $\omega_L = -2E$, $\omega_L T_{\rm on}/2\pi = 5$, $\omega_L T_D/2\pi = 105$, and $\omega_L T_{\rm off}/2\pi = 5$. The initial phase of the pulse has been chosen randomly.

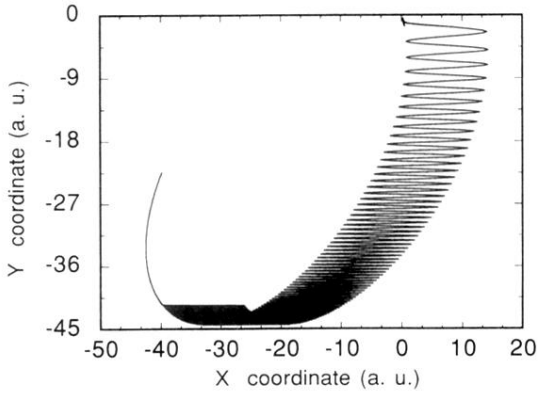

FIG. 12. Trajectory of an electron (x and y coordinates) trapped in the 3D Coulomb potential. Parameters are the same as in Fig. 11.

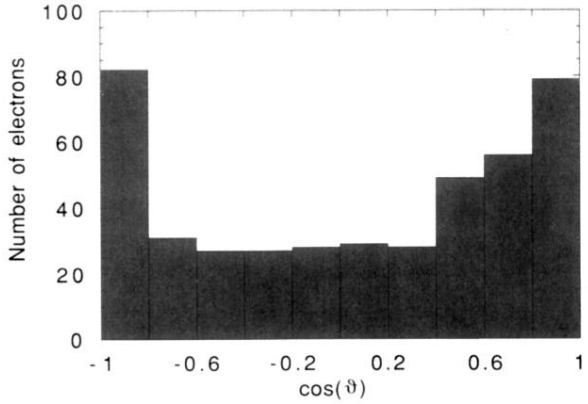

FIG. 24. Angular distribution of ionized electrons for the case of regularized potential with $\epsilon = 1$. We present the number of electrons as a function of the cosine of the angle between the final velocity and polarization axis. The parameters of the pulse are the same as in Fig. 18.

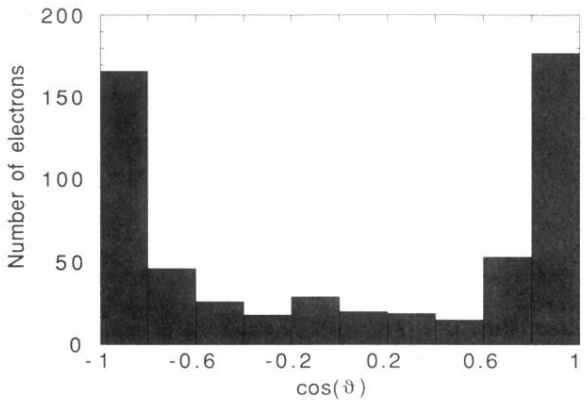

FIG. 25. Angular distribution of ionized electrons for the case of a regularized potential with $\epsilon = 1$. The parameters of the pulse are the same as in Fig. 18, except $\mathcal{E}_L = 2$.

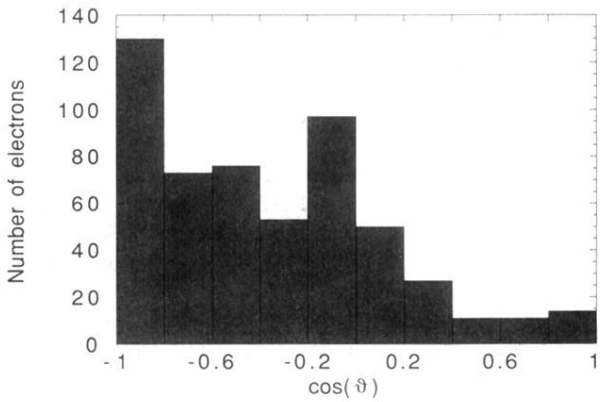

FIG. 26. Angular distribution of ionized electrons for the case of Coulomb potential. The parameters of the pulse are the same as in Fig. 18.

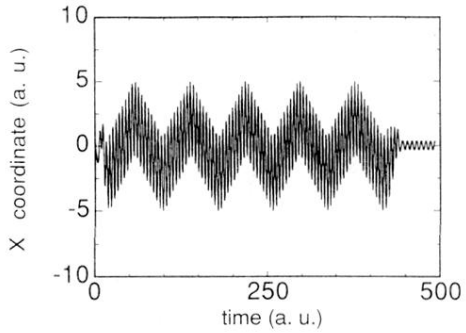

FIG. 3. Trajectory of an electron (x coordinate) trapped in the regularized 1D potential as a function of time. Parameters are the same as in Fig. 1.

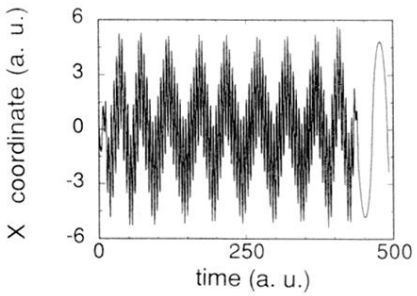

FIG. 4. Another example of a trajectory of an electron (x coordinate) trapped in the regularized 1D potential as a function of time. Parameters are the same as in Fig. 1.